Purdue University

Purdue e-Pubs

CTRC Research Publications

Cooling Technologies Research Center

3-1-2023

# Performance optimization by adaptive control of material properties in portable electronic devices

S. Bandyopadhyay

Justin Weibel
jaweibel@purdue.edu

Follow this and additional works at: https://docs.lib.purdue.edu/coolingpubs

Bandyopadhyay, S. and Weibel, Justin, "Performance optimization by adaptive control of material properties in portable electronic devices" (2023). *CTRC Research Publications.* Paper 398.
http://dx.doi.org/https://doi.org/10.1109/TCPMT.2022.3225343

This document has been made available through Purdue e-Pubs, a service of the Purdue University Libraries.
Please contact epubs@purdue.edu for additional information.

# Performance Optimization by Adaptive Control of Material Properties in Portable Electronic Devices

Soumya Bandyopadhyay and Justin A. Weibel

*Abstract*—**We evaluate the potential benefits of using tunable material properties within portable electronic devices for increasing the total power generated across different operating scenarios. In these devices, in addition to the die temperature limits, the user-exposed device skin must be kept within ergonomic comfort limits, requiring adaptive control to balance these constraints. Present thermal management strategies rely on control of the allowed amount of heat generation (performance throttling) to maintaining the die and skin temperatures within permissible limits as the operating conditions fluctuate. To address this drawback, we investigate the performance benefits offered by integration of material layers into a representative device that could adaptively control their properties, so as to maximize the heat dissipation while preserving the junction and skin temperatures within prescribed bounds. A steady-state model is employed to identify the required thermal conductivity of the tunable material layers that maximize the device performance. The model predicts that tunable materials could offer a ~15-20% increase in the maximum power that can be dissipated, owing to modulation of the junction–to-skin thermal resistance, for a representative platform and range of operating conditions. We demonstrate a case study to understand the effect of introduction of the tunable material on the junction temperature at the peak power dissipation, considering the same upper and lower bounds of thermal conductivity for different device form factors. In summary, the work critically identifies the need for target material properties required to achieve this optimal performance with realistic and modest tuning ratios of the effective material conductivity, which can be used to target future materials development and controls strategies for this application.**

***Index Terms***—portable electronics, ergonomics, tunable materials, junction, skin

NOMENCLATURE

| | |
|---|---|
| $e$ | error in signal |
| $h$ | heat transfer coefficient |
| $k$ | thermal conductivity |
| $Q$ | heat input |
| $R$ | thermal resistance |
| $t$ | total device thickness |
| $T$ | temperature |
| $T_\infty$ | ambient air temperature |
| *Subscripts* | |
| $l$ | layer |
| *cond* | conduction |
| *conv* | convection |
| *cov* | cover |
| *dis* | display |
| *ip* | in-plane |
| *ja* | junction-to-ambient |
| *js* | junction-to-skin |
| *limit* | maximum allowable value |
| *mb* | motherboard |
| *sa* | skin-to-ambient |
| *sp* | spreading |
| *set* | *set point* |
| *tp* | through-plane |
| 1 | domain 1 |
| 2 | domain 2 |

The authors are with the School of Mechanical Engineering, Purdue University, West Lafayette, IN 47907 USA. (e-mail: bandyop0@purdue.edu; jaweibel@purdue.edu).

## I. INTRODUCTION

Recent advances in the capability and expectations of portable electronic devices pose significant thermal challenges, which can be detrimental to device performance and user experience if not properly managed. Sekar [1] highlighted the importance of thermal challenges, arising from the increase in power densities and intrinsic complexity of portable electronic devices, despite the significant progress made towards developing power-optimized designs and power management techniques from an electrical and software perspective. Moon *et al.* [2] evaluated passive thermal solutions, ranging from the package-level to system-level, aimed towards augmenting the thermal design power (TDP), for a given handheld device. Park *et al.* [3] proposed a use-satisfaction-oriented thermal management strategy by sacrificing the performance of the background apps to maintain the quality of the foreground apps. Hang and Kabbani [4] reviewed the thermal challenges in mobile devices and acknowledged the limitations on the maximum dissipated power given existing thermal management solutions. While the thermal management of portable electronics is important in the typical context of device reliability and performance of the integrated electronic devices, user comfort is also a significant factor, thereby introducing ergonomic design constraints. Lee *et al.* [5] introduced an adaptive thermal property control technique for simultaneous control of the device junction and skin temperatures, preventing early false throttling of device performance. In this context, tunable thermal materials were demonstrated to be instrumental in adapting a portable electronic device to its operating environment while ensuring user comfort and safety.

Tunable technologies have displayed significant potential for use in various engineering systems and, as reviewed previously [6], span a wide range of applications from solid-state refrigeration and waste heat recovery to spacecraft, electric vehicles, and power electronics. Several examples relevant to the current study focus on technologies that modulate the path of heat flow for thermal management applications. Miner *et al*. [7] introduced a thermo-electro-mechanical cooler that utilizes mechanical contact-based modulation of heat transfer rates in super-cooled pulsed thermoelectric cycles. Mckay and Wang [8] experimentally demonstrated methods to mechanically modulate thermal impedance, resulting in pulsed heat transfer and consequently enhancing thermal energy conversion. Tunable vapor chambers were experimentally fabricated by Zhou *et al.* [9] to control the rate and direction of heat flow between battery packs and the ambient in electric vehicles. Ando *et al.* [10] developed a mechanism for tuning of the thermal conductance by reversible melting and solidification of paraffin, in spacecraft. Recently, Yang *et al.* [11,12] experimentally demonstrated the modulation of thermal conductance using actuation of millimeter-scale liquid metal droplets for power electronics applications. This literature review identifies those previous investigations of tunable materials have not been expressly targeted, developed, or demonstrated for maintaining the junction and skin temperature within prescribed thresholds [4] as is critical in portable electronic devices.

The present study evaluates the potential power dissipation benefits and required thermal conductivity of tunable materials for maximizing the power dissipated by a portable electronic device under different operating conditions. The tunable material properties that maximize the dissipated power, while maintaining the junction and skin temperatures below their thresholds, are identified for a range of operating conditions. After the representative device layout is introduced, a steady-state model is introduced that is used to estimate

the effect of variable conductivities of a tunable material layer inserted at different locations. The effect of the layer tuning on the maximum dissipated power relative to the baseline configuration is discussed, and the optimal properties identified for different operating conditions. Finally, the model framework is used to optimize the increased power dissipation possible from a device under the usage of a tunable material.

## II. Approach

A steady state model for heat conduction in a representative portable device architecture is used to assess the performance benefits of inserting a tunable material. Figure 1a depicts the exploded layout for a generic portable electronic device. The motherboard, having the electronic system-on-chip (SoC)s packages, is adjacent to the battery. The motherboard interfaces with the front display and back cover of the device through intermediate supporting frames and heat spreaders. Air gaps present between the motherboard and the battery inhibit the lateral flow of heat from the electronic SoCs on the motherboard. Hence, based on the primary paths of heat flow, the model only considers conduction within the reduced stackup shown in Figure 1b, not considering the battery. The lateral dimensions of the layers in domain 1 and domain 2 are 183 mm × 54.65 mm. The assumed thicknesses and material properties of each layer are summarized in Table 1.

In the present study, heat generation from only one primary electronic SoC is considered; the analytical conduction modeling approach can be trivially extended to consider heat generation from other SoCs by superposition. It is assumed that the portable device dissipates heat to air at a reference temperature ($T_{\infty,1} = T_{\infty,2} = 300$ K) from the exposed surfaces of the display unit and the cover. Taking the baseline case having multiple air layers, we envisage that the hypothetical tunable material would be located in these available gaps of the reduced stackup. The thermal conductivity of these layers that maximizes the heat dissipation within junction and skin temperature limits are evaluated for two limiting operating scenarios: *i*) when the exposed surfaces of the display and cover dissipate heat to quiescent air, resulting in an approximate effective convective heat transfer coefficient $h_1 = h_2 = 12$ W/m$^2$K; and *ii*) when there are moderate forced convection effects, resulting in an approximate effective convective heat transfer coefficient of $h_1 = h_2 = 21$ W/m$^2$K. Details of the modeling approach and material property optimization are described in the subsections that follow.

| Layer (Domain) | Thickness (mm) | $k_{ip}$ (W/mK) | $k_{tp}$ (W/mK) |
|---|---|---|---|
| Display Unit (1) | 3 | 1.3 | 1.3 |
| Air or Material (1) | 0.6 | 0.028 | 0.028 |
| Spreader (1) | 0.15 | 386 | 386 |
| Frame (1) | 0.8 | 159 | 159 |
| Air or Material (1) | 0.3 | 0.028 | 0.028 |
| Motherboard (1) | 0.8 | 20 | 0.3 |
| Air or Material (2) | 0.32 | 0.028 | 0.028 |
| Spreader (2) | 0.15 | 386 | 386 |
| Cover (2) | 0.9 | 0.3 | 0.3 |

**Table 1** Layer thicknesses, in-plane thermal conductivity, and through-plane thermal conductivity of the material layers in the portable electronic device.

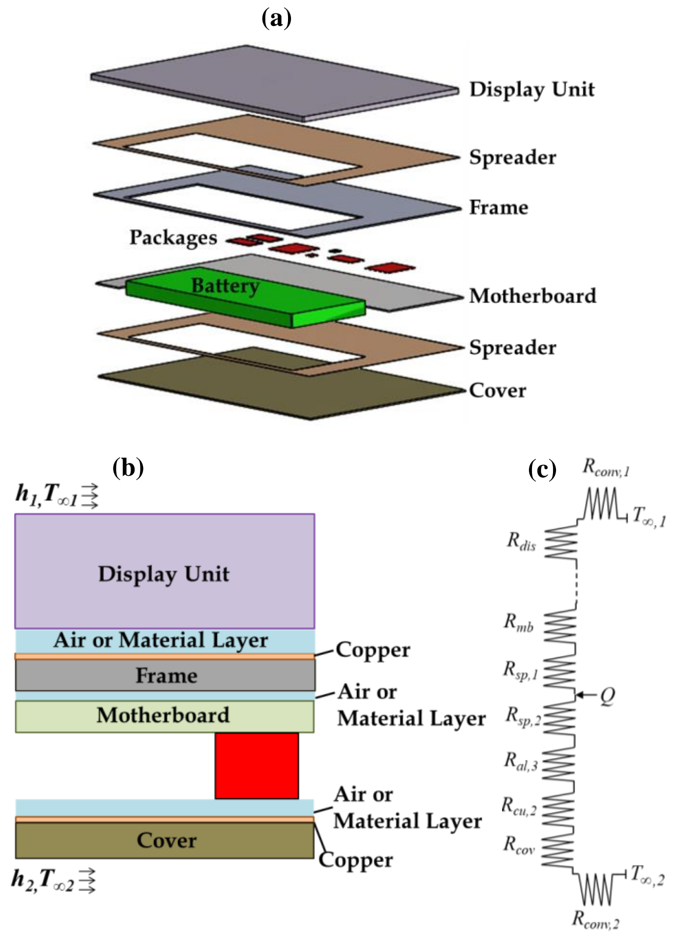


**Fig. 1** (a) Exploded drawing of a representative portable electronic device. (b) Cross-sectional schematic drawing of the reduced stackup of components in the primary heat rejection pathway, with boundary conditions indicated (not to scale). (c) Thermal resistance network of the conduction and spreading resistances considering in the multi-layer stackup.

### *A. Steady State Resistance Network*

Models are available for the exact analytical prediction of the thermal resistance for steady-state heat conduction through multi-layer stacked substrates with arbitrarily located heat inputs [13,14]. The resistance between the average junction temperature and ambient ($R_{ja}$) arises from the junction-to-skin ($R_{js}$) and skin-to-ambient ($R_{sa}$) resistances. The skin-to-ambient resistance is solely attributed to the convection resistance ($R_{conv}$) estimated from the effective convection heat transfer coefficient and the cross-sectional area of the substrate exposed to the ambient. The junction-to-skin resistance considers multi-dimensional conduction in the stackup. The resistance is broken down into a one-dimensional conduction resistance ($R_{cond}$) for each layer, computed based on the total cross-sectional area, thickness, and the thermal conductivity of each stacked layers. The spreading resistance ($R_{sp}$) accounts for the additional temperature rise at the heat source due to lateral heat flow, and is calculated from an exact Fourier-series-based analytical solution [14] of the temperature fields in a stackup comprising multiple substrates with different in-plane and through-plane thermal conductivities, subjected to a convective boundary condition. The net resistance between the junction to ambient is computed by adding the spreading, conduction, and convection resistances ($R_{ja} = R_{sp} + R_{cond} + R_{conv}$).

In the reduced device layout, the heat generated by the SoC is assumed to be spatially uniform. The equivalent network of the device (see Figure 1c) considers the bi-directional heat flow from the SoC to the front display (domain 1) and from the SoC to the back cover (domain 2), where the spreading, one-dimensional conduction, and convection resistances are estimated as outlined above. For a given total heat load ($Q$), the resistance network can be solved to yield the average junction ($T_j$) and the device skin temperatures, corresponding to the top surface of the display ($T_{s,1}$) and the cover ($T_{s,2}$).

*B. Performance Optimization*

We identify the optimal thermal properties of the material present in the air layers in the stackup, using the representative steady-state thermal network model, with an objective to maximize the dissipated heat load subject to junction and skin temperature constraints. For simplicity, it is assumed that the material present in two air layers above the motherboard in domain 1, have same thermal conductivity ($k_{al,1}$), but that this can differ from the conductivity of the material in domain 2 ($k_{al,2}$). Furthermore, it is assumed that these layers are isotropic (i.e., same thermal conductivity in the in-plane and through-plane directions). For any given combination of conductivities $k_{al,1}$ and $k_{al,2}$ there is a maximum dissipated the load ($Q_{max}$) at which either the junction or skin temperature constraints is reached. To identify the optimal pair of conductivities, $k_{al,1}$ and $k_{al,2}$, a simple optimization procedure is performed wherein this maximum heat load is predicted for all possible combination of these two conductivities. The optimal property combination is then manually identified as the one that maximizes this maximum dissipated total heat load ($Q_{max,opt}$), which is observed to always occur when both temperature constraints at met at the same heat load, at one unique property combination that presents itself as the global optimum. In this study, the respective junction and skin temperatures limits [15] are 69 ℃ and 43 ℃. Note that the optimal properties depend on the effective external convection resistance, and so this optimization process is repeated for both operating conditions *i*) and *ii*). For a given operating condition, the optimized maximum heat load ($Q_{max,opt}$) will correspond to a unique pair of optimum conductivities $k_{al,1,opt}$ and $k_{al,2,opt}$.

## III. Results

Predictions from the steady state model are first presented for the baseline thermal characteristics of the device. Then the optimum thermal conductivities of the tunable material are estimated for the range of operating conditions to understand the effect of a tunable layer on the maximum dissipated power.

*A. Baseline Performance*

The bar chart in Figure 2 compares the different components of the junction-to-ambient thermal resistance of domains 1 and 2, for the two different convective heat transfer coefficient operating conditions of the device. These results are shown for the baseline case with air layers ($k_{al,1} = k_{al,2} = 0.028$ W/mK). The overall junction-to-ambient resistances are observed to reduce with an increase in the effective convective heat transfer coefficient, as expected, due to the reduction of the skin-to-ambient resistance. This notably reveals that any given change in the external heat transfer coefficient will directly affect the skin temperature (with respect to the constant ambient temperature) for a given total heat load. A higher effective external convection coefficient will increase the skin temperature but reduce the junction temperature. This behavior motivates the need for a tunable resistance in the stackup to ensure the skin temperature remains below its limit with a change in operating conditions, by modulating the junction-to-skin resistance to counteract any changes in the skin-to-ambient resistance.

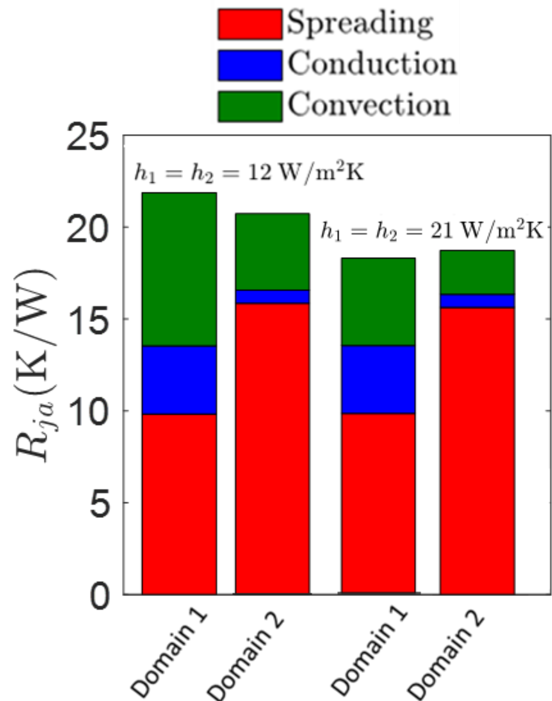


**Fig. 2** Spreading, one-dimensional conduction, and convection components of the total junction–to-ambient thermal resistance for domain 1 and domain 2 of the baseline stackup ($k_{al,1}$ = 0.028 W/mK; $k_{al,2}$ = 0.028 W/mK).

*B. Optimum Layer Properties*

The simultaneous optimization of the thermal conductivity of the tunable layers in domain 1 and domain 2 yields the respective target properties $k_{al,1,opt}$ = 0.028 W/mK and $k_{al,2,opt}$ = 0.094 W/mK when $h_1 = h_2$ = 12 W/m$^2$K. The optimal properties for $h_1 = h_2$ = 21 W/m$^2$K are $k_{al,1,opt}$ = 0.184 W/mK and $k_{al,2,opt}$ = 0.26 W/mK. These optimal conductivities set the target span of the material properties of the tunable layers for this representative device and range of operating boundary conditions. The range of optimum conductivities span less than an order of magnitude, which is therefore promising that they are achievable targets for tunable materials development. The bar chart in Figure 3 depicts the different components of the total resistance corresponding to these optimum layer properties. In these cases, the reduction in the effective convective resistance, with an increase in the heat transfer coefficient, is balanced by a reduction in the spreading and the conduction junction-to-skin resistances, thereby maintaining the junction and skin temperatures fixed at their prescribed limits.

Figure 4 plots the variation of the maximum power dissipated by the device, and the associated junction and skin temperatures, with respect to the thermal conductivity of the tunable layers in domain 1. These figures illustrate the interplay between maximum device power, the junction temperature, and the skin temperature. In this context, the conductivity of the tunable layer in domain 2 is fixed at $k_{al,2,opt}$ = 0.26 W/mK, and the operating condition is $h_1 = h_2$ = 21 W/m$^2$K. As the conductivity of the tunable layers in domain 1 is increased from the baseline of 0.028 W/mK, the maximum dissipated power of the portable electronic device increases till the optimal value of $k_{al,1,opt}$ = 0.184 W/mK. As shown in Figure 4b, for this range of properties, the maximum dissipated power corresponds to a situation for which the junction ($T_j$) and the cover temperatures ($T_{s,2}$) are at their prescribed limits, $T_{j,limit}$ and $T_{s,limit}$ respectively, but the temperature at the top surface of the display ($T_{s,1}$) remains below the skin temperature limit. This operation below the temperature limits represents an opportunity for further increasing the maximum power dissipation by increasing

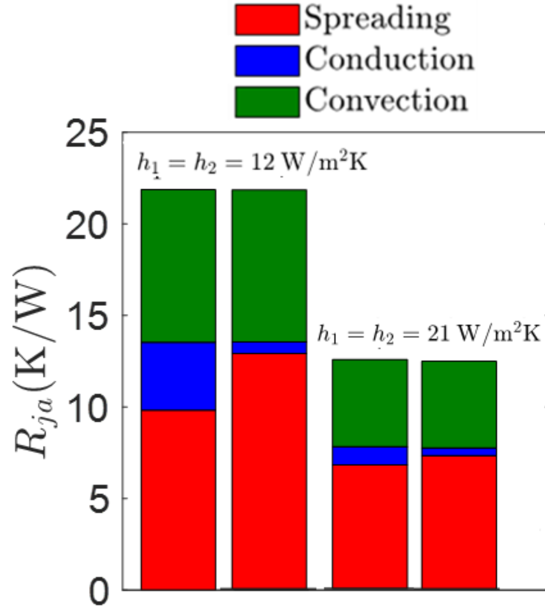


**Fig. 3** Spreading, one-dimensional conduction, and convection components of the total junction-to-ambient thermal resistance corresponding to domain 1 and domain 2. The material layer properties are tuned to maximize the heat dissipation while maintaining junction and skin temperature limits for different operating conditions: i) $k_{al,1,opt}$ = 0.028 W/mK and $k_{al,2,opt}$ = 0.094 W/mK for $h_1 = h_2$ = 12 W/m$^2$K; ii) $k_{al,1,opt}$ = 0.184 W/mK and $k_{al,2,opt}$ = 0.26 W/mK for $h_1 = h_2$ = 21 W/m$^2$K.

$k_{al,1}$, which increases $T_{s,1}$ due to the reduction in junction-to-skin resistance in domain 1. When $k_{al,1} = k_{al,1,opt}$ = 0.184 W/mK, all of the junction and skin temperatures are at their limits, which corresponds to a globally optimized maximum power ($Q_{max,opt}$ = 6.72 W).

As the conductivity of the tunable layers in domain 1 is increased beyond this optimum value, the total junction-to-ambient resistance in domain 1 becomes lower relative to the alternate heat dissipation pathway through domain 2. Consequently, for a given total heat input, the fraction of total heat flow in domain 1 would increase. Hence, the device cannot dissipate a total power greater than 6.72 W, as the display skin temperature ($T_{s,1}$) would then exceed the prescribed threshold ($T_{s,limit}$). Consequently, this results in the reduction of the maximum dissipated power with further increases in $k_{al,1}$. For $k_{al,1} > k_{al,1,opt}$, the temperature at the top surface of the cover ($T_{s,2}$) and junction temperature decrease below their limits, as the dissipated power must be reduced to ensure that the temperature at the top surface of the display ($T_{s,1}$) does not exceed its permissible limit.

### C. *Effect of Material Property Tuning on Device Performance*

To illustrate the practical performance benefit of modulating the layer thermal conductivities, Figure 5 plots the variation of the temperatures of the junction and the top surface of the display with respect to the total heat load ($Q$). For this demonstration, the conductivity of the tunable layer in domain 2 is fixed at the optimum ($k_{al,2,opt}$) values of 0.094 W/mK for $h_1 = h_2$ = 12 W/m$^2$K (Figure 5a) and 0.26 W/mK for $h_1 = h_2$ = 21 W/m$^2$K (Figure 5b). When the conductivity of tunable layers in domain 1 is at its optimum value for each case, plotted in the darker line shades, the maximum operating power corresponds a condition when the junction and skin temperatures are simultaneously at their limits. For example, when $h_1 = h_2$ = 12 W/m$^2$K in Figure 5a, the maximum dissipated power ($Q_{max,opt}$) is 3.84 W. Now suppose that under these same boundary conditions the conductivity of the layers in domain 1 is off-optimal

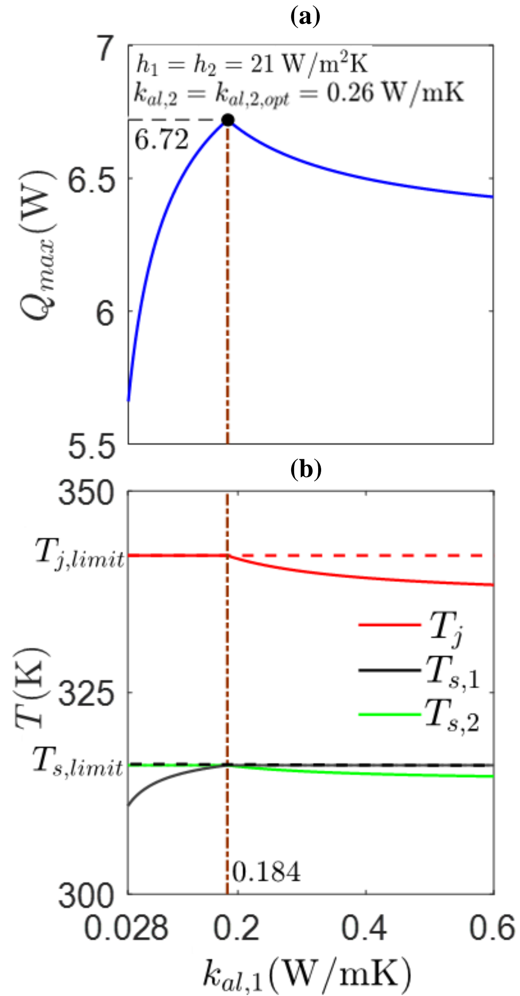


**Fig. 4** (a) Maximum dissipated power and (b) junction/skin temperatures as a function of the thermal conductivity of tunable layer in domain 1 ($k_{al,1}$), for a given operating condition ($h_1 = h_2$ = 21 W/m$^2$K) and fixed conductivity of tunable layer in domain 2 ($k_{al,2,opt}$ = 0.26 W/mK). The nomenclature $T_j$, $T_{s,1}$, and $T_{s,2}$ respectively denote the temperatures of the junction, the surface (skin) of the display, and cover. The maximum allowable temperature of the junction ($T_{j,limit}$) and the skin ($T_{s,limit}$) are 342 K and 316 K, respectively.

($k_{al,1} \neq k_{al,1,opt}$) and set to $k_{al,1}$ = 0.184 W/mK (which is the optimal value corresponding to the higher external convection case). This results in a reduction of the maximum dissipated power from 3.84 W to 3.34 W, as indicated by the lighter shaded lines in Figure 5a, at which the temperature of the top surface of the display has reached its maximum allowable limit.

In Figure 5b, for $h_1 = h_2$ = 21 W/m$^2$K, the maximum dissipated power is 6.72 W at $k_{al,1,opt}$ = 0.184 W/mK. However, if the optimal value from the lower convection coefficient case is instead considered, the maximum power dissipated by the device reduces from 6.72 W to 5.66 W due to the junction temperature reaching its permissible threshold before the skin. This pair of cases showcases the need for tuning of material properties within the device to achieve the maximum power dissipation across different operating conditions, owing to the modulation of the junction–to-skin resistance to balance multiple temperature constraints.

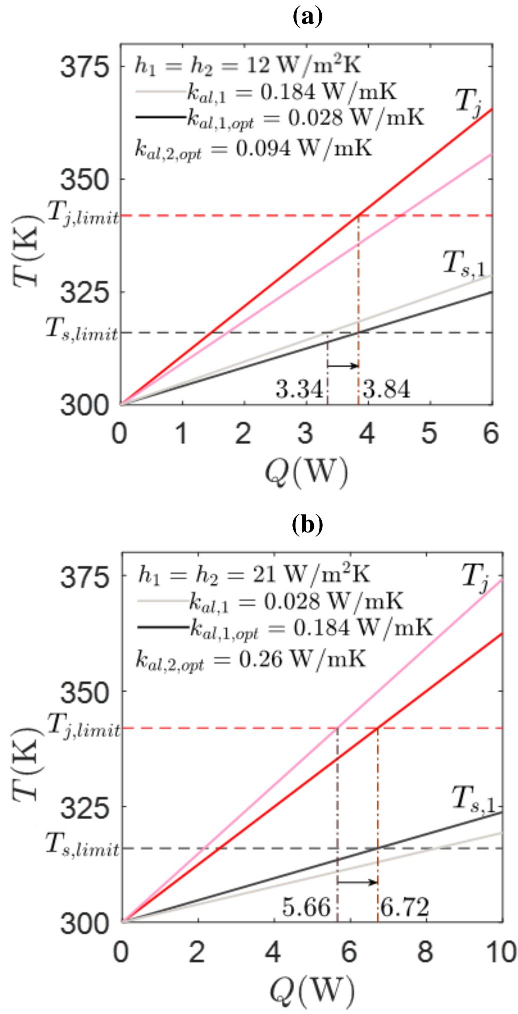


**Fig. 5** Junction ($T_j$) and display skin ($T_{s,1}$) temperatures as a function of the total dissipated power, plotted for the operating conditions: (a) $h_1 = h_2$ = 12 W/m$^2$K and (b) $h_1 = h_2$ = 21 W/m$^2$K. The thermal conductivity of tunable layer in domain 2 is fixed at the optimal value ($k_{al,2,opt}$) for each case. The maximum allowable temperature of the junction ($T_{j,limit}$) and the skin ($T_{s,limit}$) are 342 K and 316 K, respectively. The darker shade lines correspond to when the conductivity of the tunable layers in domain 1 are at their optimal for the given case, and the lighter shade lines when this conductivity is instead taken as the optimal from the other case.

*Effect of Material Property Tuning on Device Performance*

To illustrate the practical performance benefit of modulating the layer thermal conductivities, Figure 5 plots the variation of the temperatures of the junction and the top surface of the display with respect to the total heat load ($Q$). For this demonstration, the conductivity of the tunable layer in domain 2 is fixed at the optimum ($k_{al,2,opt}$) values of 0.094 W/mK for $h_1 = h_2$ = 12 W/m$^2$K (Figure 5a) and 0.26 W/mK for $h_1 = h_2$ = 21 W/m$^2$K (Figure 5b). When the conductivity of tunable layers in domain 1 is at its optimum value for each case, plotted in the darker line shades, the maximum operating power corresponds a condition when the junction and skin temperatures are simultaneously at their limits. For example, when $h_1 = h_2$ = 12 W/m$^2$K in Figure 5a, the maximum dissipated power ($Q_{max,opt}$) is 3.84 W. Now suppose that under these same boundary conditions the conductivity of the layers in domain 1 is off-optimal ($k_{al,1} \neq k_{al,1,opt}$) and set to $k_{al,1}$ = 0.184 W/mK (which is the optimal value corresponding to the higher external convection case). This results in a reduction of the maximum dissipated power from 3.84 W to 3.34 W, as indicated by the lighter shaded lines in Figure 5a, at which the temperature of the top surface of the display has reached its maximum allowable limit.

In Figure 5b, for $h_1 = h_2$ = 21 W/m$^2$K, the maximum dissipated power is 6.72 W at $k_{al,1,opt}$ = 0.184 W/mK. However, if the optimal value from the lower convection coefficient case is instead considered, the maximum power dissipated by the device reduces from 6.72 W to 5.66 W due to the junction temperature reaching its permissible threshold before the skin. This pair of cases showcases the need for tuning of material properties within the device to achieve the maximum power dissipation across different operating conditions, owing to the modulation of the junction–to-skin resistance to balance multiple temperature constraints.

*E. Effect of Material Property Tuning for Different Device Form Factors*

To assess the practical performance benefit of modulating the layer thermal conductivities for different device form factors, Figure 6 plots the variation of the temperatures of the junction with respect to the total thickness of the device. For this demonstration, the thickness of the air layer above the motherboard is varied to understand the effect of introduction of a tunable material into this layer with upper and lower bounds of conductivity to be 0.26 and 0.028 W/mK, respectively, on the device performance and junction temperatures for $h_1 = h_2$ = 12 W/m$^2$K. Under these conditions, the conductivity of the tunable layer in domain 2 ($k_{al,2,opt}$) is optimized to maintain the temperature of the display and the cover at 316 K, which is the maximum allowable temperature. The corresponding optimum conductivity of tunable layer in domain 1 ($k_{al,1,opt}$) is 0.028 W/mK. The optimum performance of the device results in a power dissipation of 3.84 W. For device thicknesses below 7.0 mm, the optimum performance results in the junction temperature below 342 K. This case highlights the fact that for device thicknesses below a particular threshold, the optimum performance does not necessarily correspond to maintaining the junction temperature at its limit considering the lower threshold of a realistic tunable material to be at the air layer conductivity.

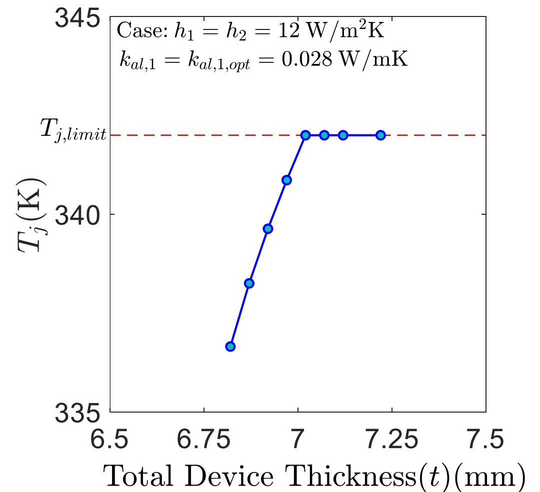


**Fig. 6** Junction ($T_j$) temperature as a function of the total device thickness ($t$), plotted for the operating conditions: $h_1 = h_2$ = 12 W/m$^2$K. The thermal conductivity of tunable layer in domain 2 ($k_{al,2,opt}$) is optimized to maintain the temperature of the display and the cover at 316 K, which is the maximum allowable temperature.

## IV. Conclusion

The power dissipation benefits and target thermal properties of including tunable thermal conductivity layers in a portable electronic device are evaluated. The hypothetical tunable material is envisaged to be applied in multiple layers inside the device, thereby allowing modulation of the junction-to-skin thermal resistance to maintain the junction and skin temperatures below their permissible limits under multiple different operating conditions. A steady-state model is used to estimate the required conductivity of the tunable material, as well as to understand the impact on the device performance. The predictions obtained from the model clearly convey the ability of a tunable material to increase the power dissipation from the device on the order of ~15-20%, with modest changes to the thermal properties (e.g., requiring less than an order of magnitude change in the effective conductance). We also assess the effect of introduction the tunable material on the device temperatures at peak performance when inserted into devices having different form factors.

The proposed approach may be generally extensible to portable electronic devices of any general form-factor, wherein there are multiple pathways of heat dissipation from an internal component to a temperature-constrained external surface. Furthermore, while the current study limited the design space exploration to isotropic material properties, available models for predicting heat spreading in anisotropic layers could be used to extend this exploration to materials having different in-plane versus through-plane thermal conductivities, with potential for further performance improvement. Lastly, while the current work identified optimal properties for a fixed operating condition, this naturally inspires the potential for dynamic control of these properties to maintain operation at the peak heat load without violating any system temperature constraints, using a controller based either an empirical model trained during device operation or a transient analytical model of the thermal system.

## References


[1] Sekar, K., 2013. Power and thermal challenges in mobile devices. 19th Annual International Conference on Mobile Computing & Networking, pp. 363-368.

[2] Moon, S.W., Prstic, S., and Chiu, C.P., 2006. Thermal management of a stacked-die package in a handheld electronic device using passive solutions. 10th Intersociety Conference on Thermal and Thermomechanical Phenomena in Electronics Systems (ITherm), pp. 791-797.

[3] Park, J., Lee, S., and Cha, H., 2018. App-oriented thermal management of mobile devices. International Symposium on Low Power Electronics and Design, pp. 1-6.

[4] Hang, Y. and Kabban, H., 2015. Thermal management in mobile devices: challenges and solutions. 31st Thermal Measurement, Modeling & Management Symposium, pp. 46-49.

[5] Lee, K.M., Im, Y., Huh, J.H., and Han, T.H., 2018. Adaptive thermal property control technique for holistic thermal management of mobile devices. IEICE Electronics Express, pp.15-20180187.

[6] Wehmeyer, G., Yabuki, T., Monachon, C., Wu, J., and Dames, C., 2017. Thermal diodes, regulators, and switches: Physical mechanisms and potential applications. Applied Physics Reviews, **4**(4), p.041304.

[7] Miner, A., Majumdar, A., and Ghoshal, U., 1999. Thermoelectromechanical refrigeration based on transient thermoelectric effects. Applied Physics Letters, **75**(8), pp.1176-1178.

[8] McKay, I.S. and Wang, E.N., 2013. Thermal pulse energy harvesting. Energy, **57**, pp.632-640.

[9] Zhou, F., Liu, Y., Joshi, S.N., Dede, E.M., Chen, X., and Weibel, J.A., 2017. Vapor chamber with thermal diode and switch functions. 16th Intersociety Conference on Thermal and Thermomechanical Phenomena in Electronic Systems (ITherm), pp. 521-528.

[10] Ando, M., Shinozaki, K., Okamoto, A., Sugita, H., and Nohara, T., 2014. Development of mechanical heat switch for future space missions. 44th International Conference on Environmental Systems.

[11] Yang, T., Kwon, B., Weisensee, P.B., Kang, J.G., Li, X., Braun, P., Miljkovic, N., and King, W.P., 2018. Millimeter-scale liquid metal droplet thermal switch. Applied Physics Letters, **112**(6), p.063505.

[12] Yang, T., Foulkes, T., Kwon, B., Kang, J.G., Braun, P.V., King, W.P., and Miljkovic, N., 2019. An integrated liquid metal thermal switch for active thermal management of electronics. IEEE Transactions on Components, Packaging and Manufacturing Technology, **9**(12), pp.2341-2351.

[13] Muzychka, Y.S., Culham, J.R., and Yovanovich, M.M., 2003. Thermal spreading resistance of eccentric heat sources on rectangular flux channels. Journal of Electronic Packaging, **125**(2), pp.178-185.

[14] Bagnall, K.R., Muzychka, Y.S., and Wang, E.N., 2014. Analytical solution for temperature rise in complex multilayer structures with discrete heat sources. IEEE Transactions on Components, Packaging and Manufacturing Technology, **4**(5), pp.817-830.

[15] Divakar, M.P., 2016. Surface temperatures of electronics products: appliances vs. wearables. Electronics Cooling. (https://www.electronics-cooling.com/2016/09/surface-temperatures-of-electronics-products-appliances-vs-wearables/)